The Vertical Structure of Wintertime Climate Regimes of the Northern Hemisphere Extratropical Atmosphere

ADAM HUGH MONAHAN

Institut für Mathematik, Humboldt-Universität zu Berlin, Berlin, Germany

JOHN C. FYFE

Canadian Centre for Climate Modelling and Analysis, Meteorological Service of Canada, University of Victoria, Victoria, British Columbia, Canada

LIONEL PANDOLFO

Department of Earth and Ocean Sciences, University of British Columbia, Vancouver, British Columbia, Canada

(Manuscript received 7 July 2001, in final form 18 July 2002)

ABSTRACT

A nonlinear generalization of principal component analysis (PCA), denoted nonlinear principal component analysis (NLPCA), is applied to Northern Hemisphere wintertime geopotential heights at 1000, 700, 500, 300, and 20 hPa. It is found that the optimal nonlinear approximation to the data at the four tropospheric levels is characterized by three equivalent-barotropic regimes of circulation. The NLPCA time series provides a kinematic description of variability within the regimes and transitions between them. The occupation frequencies of the regimes demonstrate substantial interannual and interdecadal variability, some of which can be associated with the influence of El Niño–Southern Oscillation. The stratospheric geopotential height field is also characterized by three circulation regimes. Two of these characterize a vacillation of polar vortex shape and polar temperature. The third regime, which is occupied episodically, is characterized by dramatic reductions in the zonal-mean zonal wind and meridional temperature gradient at high latitudes, and is associated with stratospheric sudden warmings. Evidence is presented for a connection between the stratospheric and tropospheric regimes, including an association between stratospheric sudden warmings and North Atlantic blocks. Finally, these results are compared to previous studies of regime structure and to the Arctic Oscillation paradigm.

1. Introduction

The idea that the low-frequency variability (LFV) of the general circulation of the extratropical Northern Hemispheric (NH) atmosphere can be characterized by a small number of preferred circulation patterns, or regimes, dates back to the pioneering work of Baur (1931) and Namias (1950) in the first half of the last century (see Pandolfo 1993, for a review). Interest in this idea was rekindled in the late 1970s with the work of Charney and DeVore (1979), which demonstrated the existence of multiple stationary states in a highly truncated model of the interaction between the extratropical general circulation and topography. Early observational evidence for the existence of multiple regimes of atmospheric circulation was presented by Sutera (1986), who demonstrated the bimodality of the probability density function (PDF) of an index measuring the amplitude of wavenumbers 2–4 of the midlatitude 500-hPa height field. Further observational evidence for the existence of regimes was provided by Kimoto and Ghil (1993), who, in an estimate of the joint PDF of the leading two modes from a principal component analysis (PCA) of the 700-hPa geopotential height field, found distinct departures from multinormality corresponding to four distinct hemispheric circulation regimes. At about the same time, Cheng and Wallace (1993) used a hierarchical cluster analysis technique to identify three preferred regimes of circulation in the NH 500-hPa flow. The clusters identified by Cheng and Wallace were in close agreement with three of the regimes diagnosed by Kimoto and Ghil. Interest in observational studies of extratropical atmospheric LFV from this nonlinear perspective was recently renewed when analyses of the 700- and 500-hPa flow by Smyth et al. (1999) and Corti et al. (1999) confirmed the results of Cheng and Wallace using distinct statistical methods (respectively, mixture-model clustering and visual inspection of the joint PDF

Corresponding author address: Dr. A. H. Monahan, School of Earth and Ocean Sciences, University of Victoria, P.O. Box 3055 STN CSC, Victoria, BC V8W 3P6, Canada.
E-mail: monahana@uvic.ca

of the leading two PCA modes), although the statistical significance of these results remains a subject of debate (e.g., Hsu and Zwiers 2001; Hannachi and O'Neill 2001; Stephenson et al. 2001, manuscript submitted to *J. Climate*). These ideas have attracted particular attention in light of the hypothesis that climate change may manifest itself in changes in the occupation statistics of preferred climate regimes (Palmer 1999).

The above studies concentrated on the diagnosis of regimes in the tropospheric circulation. Pierce and Fairlie (1993) reported evidence of the existence of three preferred circulation regimes in the NH extratropical wintertime stratosphere, through a consideration of the PDFs of geopotential height wavenumber 1 and the zonal-mean zonal wind at 100 and 10 hPa. To our knowledge, this is the only observational evidence for multiple regimes of stratospheric circulation so far presented in the literature.

Parallel to the above nonlinear statistical analyses, a large number of studies of extratropical atmospheric LFV using linear statistical approaches were carried out. Statistical techniques used included correlation analysis and PCA (e.g., Wallace and Gutzler 1981), rotated PCA (e.g., Barnston and Livezey 1987), singular value decomposition (e.g., Wallace et al. 1992), and canonical correlation analysis (e.g., Perlwitz and Graf 1995). These analyses highlighted a number of characteristic structures of variability such as the North Atlantic Oscillation (NAO) and the Pacific–North America (PNA) pattern, each of which consists of a fixed spatial pattern modulated by a time series that fluctuates in amplitude and sign. Recently, a considerable amount of interest has been focused on one of these structures: the Arctic Oscillation (AO) or annular mode (Thompson and Wallace 1998, 2000), which emerges as the leading mode of a principal component analysis of NH extratropical geopotential heights. The AO has attracted attention for a number of reasons: it appears to be a hemispheric generalization of the NAO, it displays considerable vertical coherence throughout the troposphere and the stratosphere, and, in particular, it displays a long-term trend that GCM studies suggest may be a dominant dynamical signal of anthropogenic climate change (Shindell et al. 1999; Fyfe et al. 1999; Thompson et al. 2000). In contrast to the regime-based analysis of extratropical NH atmospheric LFV, an inherently linear view of atmospheric LFV underlies these linear statistical studies.

Most recently, evidence for the existence of preferred regimes of atmospheric circulation has been obtained using a nonlinear generalization of PCA, denoted nonlinear principal component analysis (NLPCA; Monahan 2000a). Whereas classic PCA produces optimal linear lower-dimensional approximations to multivariate data, NLPCA is able to characterize more general nonlinear low-dimensional structure. In a long integration of the Canadian Centre for Climate Modelling and Analysis (CCCma) coupled general circulation model (CGCM) with CO_2 and aerosol forcings at preindustrial levels, NLPCA was able to demonstrate the existence of multiple regimes of variability in the monthly averaged wintertime NH extratropical sea level pressure and 500-hPa geopotential height fields (Monahan et al. 2000, hereafter MFF; Monahan 2000b). A subsequent analysis of an integration with CO_2 and aerosol forcings at the projected year 2100 levels demonstrated that the dominant dynamical effect of these changes in forcing was a substantial depopulation of one of the circulation regimes, consistent with the hypothesis of Palmer (1999). When applied to the observed daily, 10-day low-pass filtered 500-hPa geopotential height field (Monahan et al. 2001, hereafter MPF), the regimes characterized in Cheng and Wallace (1993), Smyth et al. (1999), and Corti et al. (1999) were recovered. However, where these previous nonlinear analyses were essentially static, the NLPCA description included both spatial and temporal information, providing a kinematic description of the regimes and the transitions between them.

In this study, we extend the analysis of MPF to an analysis of geopotential heights throughout the depth of the troposphere and up into the stratosphere. It will be shown that the regime structure found at 500 hPa is equivalent barotropic throughout the troposphere, but that the structure of stratospheric regimes is rather different. This result stands in contrast to the AO description of extratropical atmospheric LFV, in which the annular modes are essentially coherent throughout both the troposphere and the stratosphere. We will argue that, in fact, the AO description in both regions arises as the optimal linear approximation to the fundamentally nonlinear structure of extratropical atmospheric LFV. Section 2 of the paper describes the datasets used and provides a brief description of NLPCA. The results of the analysis of the tropospheric and stratospheric datasets are presented in sections 3 and 4, respectively. A discussion and conclusions are presented in section 5.

2. Data and methodology

The data used in this analysis are twice-daily boreal wintertime (December–February, hereafter DJF) geopotential heights at 1000, 700, 500, 300, and 20 hPa, and temperature at 20 hPa, from the National Centers for Environmental Prediction–National Center for Atmospheric Research (NCEP–NCAR) reanalysis dataset (Kalnay et al. 1996), for the period 1958–98. These were averaged to daily values and subsampled from the original $2.5^\circ \times 2.5^\circ$ grid to a $5^\circ \times 5^\circ$ grid. An annual cycle was calculated for each field in the same manner as in Smyth et al. (1999), and anomaly fields were defined relative to this annual cycle. These anomaly fields were further smoothed using the 10-day low-pass filter of Wallace et al. (1988). The dataset thus consists of a set of 3670 daily maps at each pressure level (41 winters, including 10 leap years, less 30 points at the beginning and end of the record due to the filtering). The 1000-

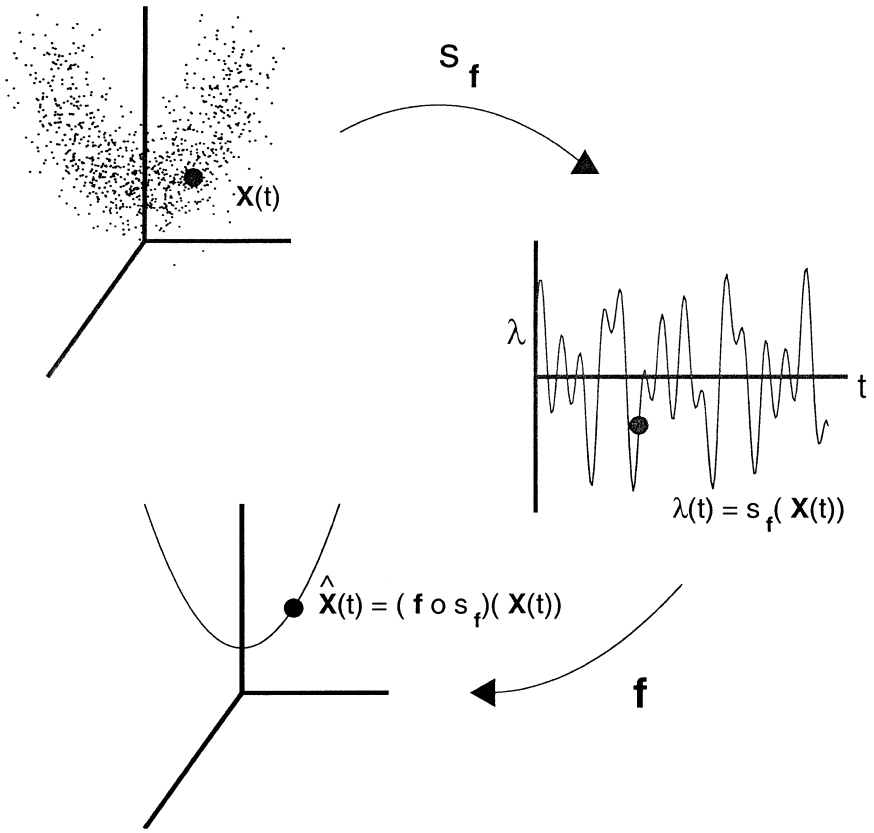

FIG. 1. Geometric representation of NLPCA.

hPa geopotential height anomaly field is denoted Z_{1000}, and similarly for the other geopotential height fields. The 20-hPa temperature field is denoted T_{20}.

To compress the data to a manageable size, a PCA was carried out at each pressure level. Before performing the PCA, the fields were weighted by the square root of the cosine of the latitude, to account for the poleward concentration of grid points. A combined PCA (CPCA) of the four tropospheric fields (1000, 700, 500, and 300 hPa) was then performed, after normalizing each field by the square root of its spatial mean variance. The resulting dataset is denoted Z_{CPCA}. The spatial maps of the leading CPCA modes, characterized by roughly zonally symmetric anomalies of opposite sign between middle and high latitudes, agree with those presented in Baldwin and Dunkerton (1999). The 20-hPa field was not included in the combined analysis because, as will be shown, it displays qualitatively different regime structure than the tropospheric fields.

These data were analyzed using the recently developed technique of NLPCA. This method and its implementation are described in detail in Monahan (2000a, 2001); a brief description follows. Given the M-dimensional dataset $\mathbf{X}(t_n)$, where each of the M dimensions corresponds to a grid point and $n = 1, \ldots, N$ labels the points in time, we look for two functions $\mathbf{s_f}: \Re^M \rightarrow \Re^P$ and $\mathbf{f}: \Re^P \rightarrow \Re^M$, $P < M$, such that the approximation

$$\hat{\mathbf{X}}(t_n) = (\mathbf{f} \circ \mathbf{s_f})[\mathbf{X}(t_n)] \tag{1}$$

is optimal in that the mean-squared difference from the original data,

$$\epsilon^2 = \langle \|\mathbf{X} - \hat{\mathbf{X}}\|^2 \rangle, \tag{2}$$

is minimized. In the above, the notation $\mathbf{f} \circ \mathbf{s_f}$ denotes the composition of the functions $\mathbf{f}$ and $\mathbf{s_f}$ {i.e., $(\mathbf{f} \circ \mathbf{s_f})(x) = \mathbf{f}[\mathbf{s_f}(x)]$}, the operator $\| \cdot \|$ denotes the L^2 norm, and the angle brackets $\langle \cdot \rangle$ denote the sample average in time. The resulting approximation $\hat{\mathbf{X}}(t_n)$ is then denoted as the P-dimensional NLPCA approximation to $\mathbf{X}(t_n)$. In the case $P = 1$, $\hat{\mathbf{X}}(t_n)$ describes a one-dimensional curve in $\Re^M$ and is denoted as the leading NLPCA mode. In the limit where the functions $\mathbf{s_f}$ and $\mathbf{f}$ are constrained to be linear, NLPCA reduces to traditional PCA.

A geometric description of NLPCA is presented in Fig. 1. The original data are presented in the upper-left-hand corner as a data cloud in some abstract Cartesian state space. This state space may be, for example, the original gridpoint space or the space of the PCA modes. The leading PCA mode of this dataset is the one-dimensional linear structure that approximates the data in an optimal manner. Clearly though, the data cloud of

Fig. 1 has an underlying *nonlinear* one-dimensional structure that cannot be described by PCA with optimal efficiency. Nonlinear PCA was developed to characterize such nonlinear structures.

In Fig. 1, the function $\mathbf{s_f}$ is shown mapping from the original data to a 1D time series $\lambda(t_n) = \mathbf{s_f}[\mathbf{X}(t_n)]$, which is then mapped by $\mathbf{f}$ to the 1D curve in the original space, $\hat{\mathbf{X}}(t_n)$. Each point on the curve $\hat{\mathbf{X}}(t_n)$ corresponds to a unique point in the time series $\lambda(t_n)$: the function $\mathbf{f}$ describes the *structure* of the approximation in the original M-dimensional state space, and $\lambda(t_n)$ describes the temporal evolution of the approximation along this structure. In formal terms, $\mathbf{f}$ is a 1D manifold embedded in $\Re^M$ and λ is the parameterization of that manifold. The large circles in Fig. 1 represent, respectively, a point in the original data and the corresponding points in the time series $\lambda(t_n)$ and on the approximation $\hat{\mathbf{X}}(t_n)$.

Because of the structure of the NLPCA approximation (1), the time series $\lambda(t_n)$ is only defined up to an arbitrary homeomorphism, that is, a one-to-one, onto, and continuous function with a continuous inverse (Monahan 2001). The most natural parameterization is by arc length: one end of the curve $\hat{\mathbf{X}}(t_n)$ is assigned the value 0 and the other end the value 1, and each point in between is assigned a value corresponding to the fraction of the length along the curve from the 0 point at which it lies. We will use this parameterization throughout this paper.

Each mode of classic PCA is assigned a unique time series and a unique spatial pattern. In NLPCA, however, while the 1D approximation is associated with a unique time series $\lambda(t_n)$, there is no unique spatial pattern. Instead, each point on the approximation $\hat{\mathbf{X}}(t_n)$ is associated with a different map. This map is easily obtained for any point on the approximation: each such point lies in the state space spanned by axes representing either grid points or PCA modes. The projection of this point on these axes describes a unique spatial pattern. Because 1D PCA approximations are produced by multiplying the associated map with the associated time series, such approximations can only describe standing variability in which the characteristic spatial structures change only in sign and amplitude. The NLPCA approximation is able to characterize more general structures of variability.

Often, PCA modes are interpreted individually, with the justification (given either implicitly or explicitly) that, by construction, these modes are temporally uncorrelated. In fact, a vanishing correlation between two variables does not imply that they are independent (although the converse is of course true). A simple illustration of this is given by the random variables x and $y = x^2$, where x is uniformly distributed between -1 and 1. The random variables x and y are uncorrelated, that is, $E(xy) = 0$, where $E(\cdot)$ denotes the expectation operator. However, x and y are clearly not independent: the conditional distribution $p(y|x)$ is not equal to the marginal $p(y)$. Nonlinear PCA is able to characterize dependence between PCA modes, should it exist, and is therefore able to produce a more representative approximation to the original data. If the physical system is imagined to evolve along an attractor, PCA may be used to characterize its embedding space, while NLPCA can characterize the attractor itself. This was demonstrated for the Lorenz system in Monahan (2000a). We do not suggest that individual NLPCA modes are mutually independent. Nonetheless, they generally produce approximations that are more representative of the data than those produced by PCA. Recently, an attempt has been made to characterize statistically independent, albeit linear, modes of climate variability (Aires et al. 2000).

In this study, NLPCA is not carried out on the original data, because of their very high spatial dimensionality, but rather on the data projected onto their leading 10 PCA modes. It is possible that some signal may be lost in this projection. However, it is found a posteriori that, in all cases considered here, the leading NLPCA modes project significantly onto only the first few PCA axes. Consequently, we are confident that it is highly unlikely that any of the signal of importance to the leading NLPCA mode has been lost in the reduction of the original data to this smaller state space. The truncation employed here is in any case much less drastic than that employed by Smyth et al. (1999) or Corti et al. (1999), in which only the state space spanned by the leading two PCA modes was considered.

3. Analysis of tropospheric geopotential heights

Separate NLPC analyses of Z_{1000}, Z_{700}, Z_{500}, Z_{300}, and Z_{CPCA} were carried out; the results of the analysis of the Z_{500} field are described in MPF. The NLPCA approximations for each of these separate tropospheric height fields are very similar to each other and to the corresponding sector of the NLPCA approximation of the CPCA field. Consequently, the following discussion will concentrate on the results of the combined analysis.

Figure 2 displays $\hat{Z}_{\mathrm{CPCA}}$, the 1D NLPCA approximation to Z_{CPCA}, as a curve in the space spanned by the leading three CPCA modes. The approximation $\hat{Z}_{\mathrm{CPCA}}$ is a mixture of CPCA modes 1, 2, and 3. The projection of $\hat{Z}_{\mathrm{CPCA}}$ onto CPCA modes higher than 3 is negligible. Also displayed in Fig. 2 are contour plots of $p(CPC_i, CPC_j) - p(CPC_i)p(CPC_j)$, $(i, j) = (1, 2), (1, 3), (2, 3)$, the differences between estimates of the joint PDF of each pair of CPCA modes and the product of estimates of the marginal distributions. If two CPCA modes were statistically independent, the joint distribution would factorize as the product of the marginals and this difference would be zero. Regions where the difference is positive (negative) correspond to parts of state space in which the system resides more (less) often than would be the case if the CPCA modes represented independent modes of variability; they are preferred (unpreferred) regions of state space. As shown in Fig. 2, the NLPCA

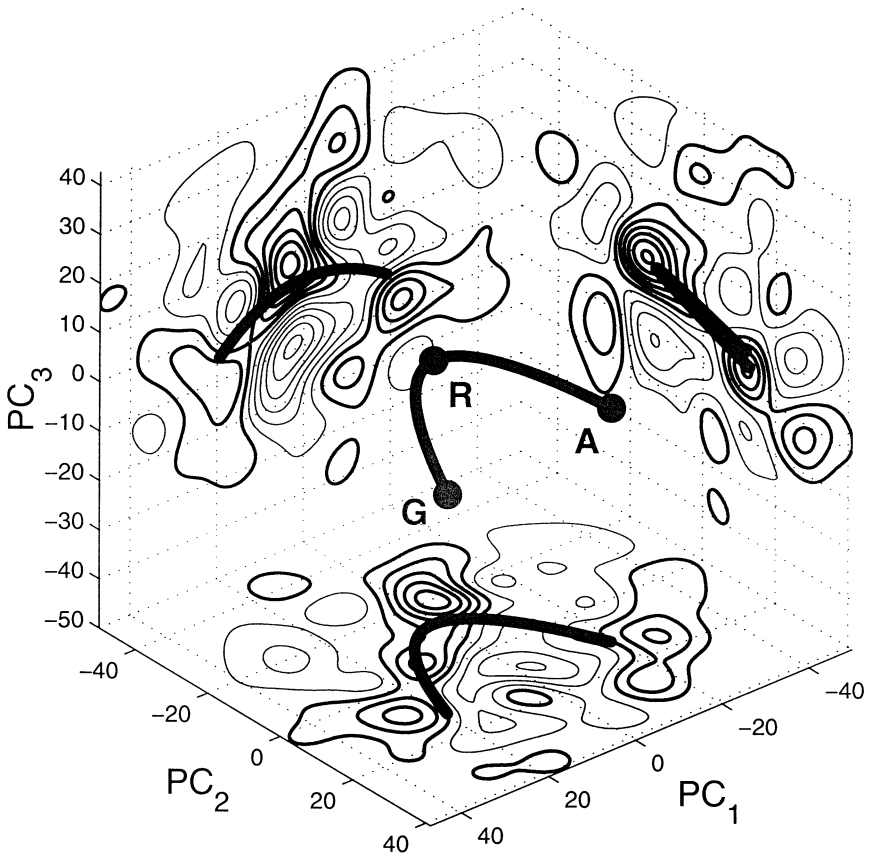

FIG. 2. Plot of the 1D NLPCA approximation $\hat{Z}_{\mathrm{CPCA}}$ (thick curve) projected onto the leading three CPCA modes. Also contoured are the difference between estimates of the joint PDF $p(\mathrm{CPC}_i, \mathrm{CPC}_j)$ of these modes and the product of the marginal PDFs $p(\mathrm{CPC}_i)\, p(\mathrm{CPC}_j)$ for each pair $(i, j) = (1, 2), (1, 3), (2, 3)$. The PDFs were estimated using a Gaussian kernel estimator with a smoothing parameter $h = 4.5$. Thick contours are positive differences and thin contours are negative. Contour interval is $(\ldots, -3, -1, 1, 3, \ldots) \times 10^{-5}$.

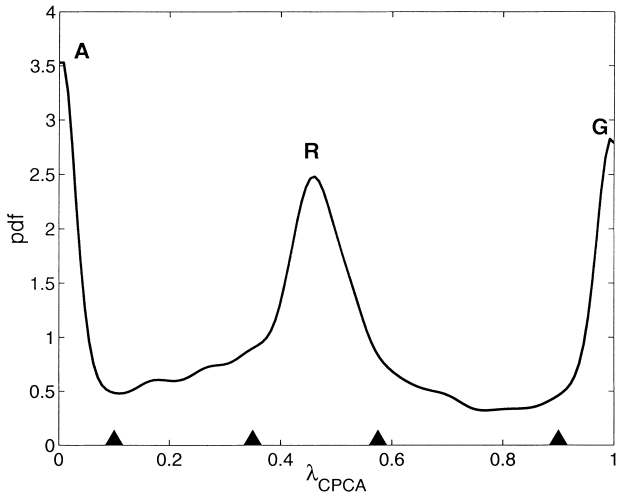

FIG. 3. Gaussian kernel estimate of the PDF of the NLPCA time series λ_{CPCA}. The estimate was made with a smoothing parameter $h = 0.025$. The triangles denote the position of the boundaries between the regimes and the transition zones.

approximation lies primarily in the preferred regions of the state space, and avoids the unpreferred regions.

Figure 3 displays an estimate of the PDF of the NLPCA time series $\lambda_{\mathrm{CPCA}}(t_n)$. As was the case with the NLPCA approximation of the 500-hPa field considered in MPF, the distribution of $\lambda_{\mathrm{CPCA}}(t_n)$ is characterized by three distinct peaks. For consistency with MPF we follow Cheng and Wallace (1993) and denote the peaks A, R, and G. These designations arise because, as will be illustrated presently, the associated spatial maps have strong positive centers of action over the Aleutians, the Rockies, and Greenland, respectively. The points on $\hat{Z}_{\mathrm{CPCA}}$ corresponding to the tops of peaks A, R, and G are denoted by the large circles in Fig. 2. As in MPF, we interpret the peaks in the PDF of $\lambda_{\mathrm{CPCA}}(t_n)$ as describing preferred regimes in the extratropical tropospheric circulation. The intervals [0, 0.1], [0.35, 0.575], and [0.9, 1] will be considered to correspond to regimes A, R, and G, respectively; the boundaries of these intervals are denoted by triangles in Fig. 3. These intervals were determined subjectively, but all of the following

results are robust with respect to reasonable changes in their boundaries.

A plot of $\lambda_{\mathrm{CPCA}}(t_n)$ for each complete winter of the dataset is presented in Fig. 4. Note that in the present study the phrase ''winter of 1960,'' for example, denotes the DJF period for which the January and February fall in 1960. Figure 4 elucidates the temporal structure of the NLPCA approximation. Two distinct timescales are involved. The shorter timescale, on the order of a few days, corresponds to rapid transitions between the regimes. The longer timescale corresponds to the period for which the approximation resides in one of the three regimes. There is in fact a broad distribution of regime residence times, as is illustrated in Fig. 5. This figure displays a histogram estimate of the probability distribution $p(T)$ of regime residence times, T, for events in which the approximation resided within a regime for at least 5 days. The distribution of T appears to be approximately exponential:

$$p(T) \simeq \frac{1}{\tau} \exp\left(-\frac{T}{\tau}\right). \tag{3}$$

Figure 5 also displays the least squares estimate of the exponential distribution (3) for the histogram; the e-folding time τ is about 18 days. Similar histograms and e-folding times are found for the occupation statistics of each regime considered individually (not shown). The exponential distribution of residence times is consistent with the description of atmospheric low-frequency variability as a dynamical system composed of multiple attractors, with transitions between attractors induced by ''noise'' associated with high-frequency variability (Gardiner 1997). Inspection of Fig. 4 also indicates that there is considerable interannual variability in the occupation statistics of the three regimes. In some winters, such as 1971, the system spends approximately equal times in each of these regimes, whereas the winters of 1969 and 1989 are dominated by regimes G and A, respectively.

As was noted in section 2, maps corresponding to the points on the NLPCA approximation $\hat{Z}_{\mathrm{CPCA}}$ can be constructed. The spatial patterns corresponding to the points A, R, and G in Fig. 2 are displayed in Fig. 6 for each of the four tropospheric pressure levels. The spatial patterns of geopotential height at 500 hPa are essentially identical to those reported in MPF for the analysis of this field alone. Clearly, $\hat{Z}_{\mathrm{CPCA}}(t_n)$ is strongly equivalent barotropic, with anomaly patterns that amplify with altitude through the troposphere.

Regimes A, R, and G have been noted as the three dominant regimes of Northern Hemisphere extratropical LFV at individual tropospheric levels in a number of studies (e.g., Cheng and Wallace 1993; Smyth et al. 1999; Corti et al. 1999). This convergence of the results of separate analyses, using different statistical techniques inspires confidence that these regimes are in fact characteristic of the NH extratropical wintertime LFV.

The spatial patterns of regimes R and A over the Pacific–North American (PNA) sector bear a strong resemblance to the positive and negative phases of the classic PNA pattern, while those of regimes R and G over the Atlantic sector resemble the positive and negative phases of the NAO. There is, however, a fundamental difference between the description of atmospheric variability in terms of the PNA–NAO and that suggested here. The PNA–NAO description imagines atmospheric low-frequency variability as being composed of a number of characteristic structures that fluctuate in amplitude and sign but not in spatial pattern, perhaps interacting to some extent among themselves, and with unimodal PDFs that do not deviate significantly from Gaussianity. This is an essentially linear view of atmospheric variability. The regime-based view, on the other hand, characterizes LFV by a number of preferred circulation states, around which the atmosphere resides for extended periods and between which it moves rapidly. This description is fundamentally nonlinear.

When interpreting Fig. 4, it is important to keep in mind that $\hat{Z}_{\mathrm{CPCA}}$ accounts for only 19% of the variance of the 10-day low-pass filtered data (slightly more than the 15% captured by PCA mode 1). The actual data contain considerable variability around the NLPCA approximation. Consequently, maps of geopotential height for individual days spent within a given regime will differ from each other, and from the average maps displayed in Fig. 6, in their detailed features. The averaged maps shown in Fig. 6 do not fully represent the instantaneous states within the corresponding regimes, but rather the centers of those parts of state space around which trajectories tend to cluster. Of course, a similar caveat holds in the consideration of the leading PCA mode: the AO explains only a small fraction of the total variance, and the real state of the atmosphere at any time may differ strikingly from its description in terms of the AO.

The frequencies of occupation of regimes A, R, and G display substantial interannual variability. Figure 7 displays the annual occupation frequencies of regimes A, R, and G, for each winter in the observational record. While for the most part this interannual variability results presumably from internal chaotic fluctuations, it is also influenced by interannual variability in the boundary forcing. In particular, Fig. 7 hints at an increased frequency of occupation of regime A during La Niña events and of regime R during El Niño events.

To demonstrate this influence of ENSO, each of the winters in the dataset was classified as an El Niño, La Niña, or ''normal'' winter, using the stratification of Renwick and Wallace (1996), updated to include the El Niño of 1998. Figure 8 displays estimates of the PDF of $\lambda_{\mathrm{CPCA}}(t_n)$ for El Niño and La Niña winters. There is an increase in the population of regime R and a decrease in population of regime A during El Niño winters, and vice versa for La Niña winters. Because the geopotential height anomalies in regimes A and R in the Pacific–

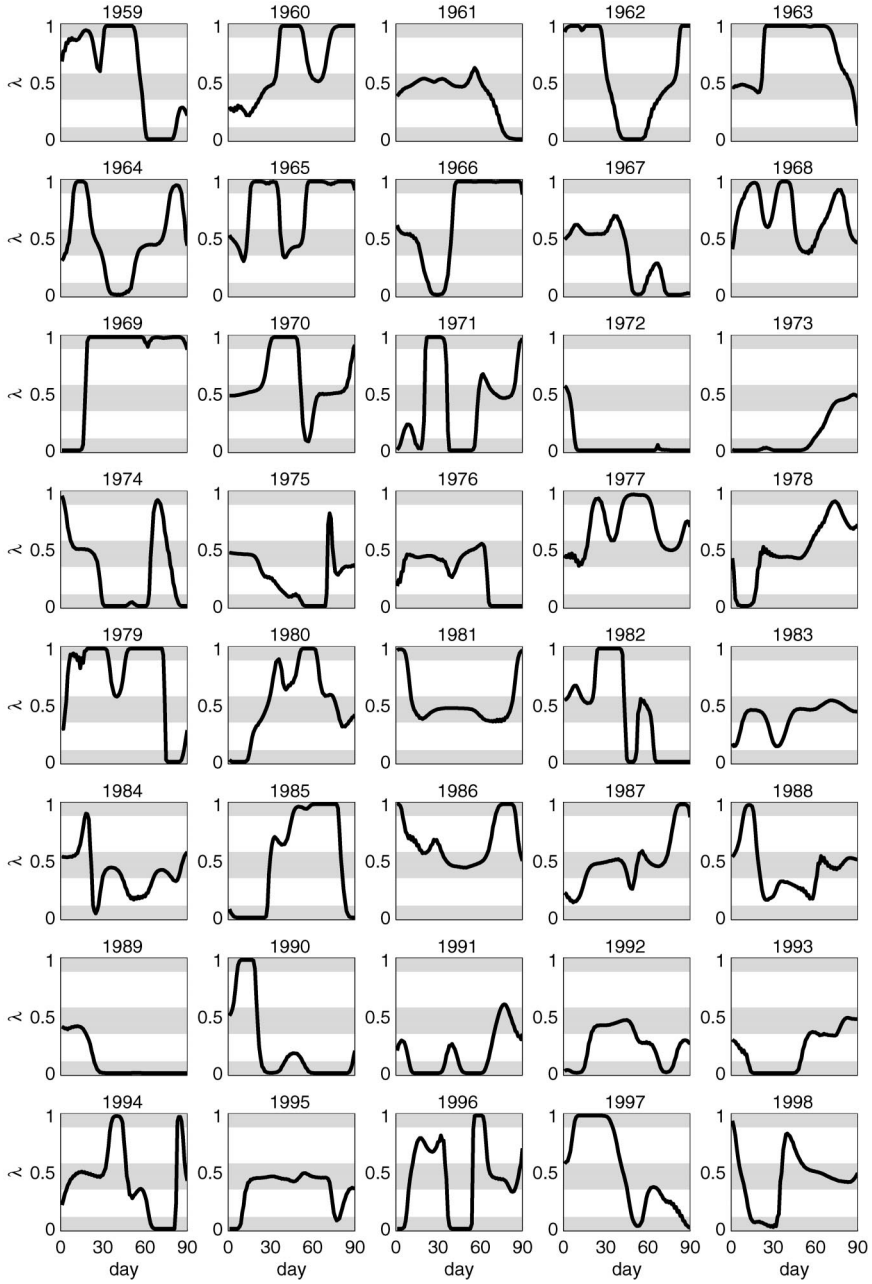

FIG. 4. Plot of the time series $\lambda_{\mathrm{CPCA}}(t_n)$ for each of the full winters considered in this study. The shaded regions denote the λ_{CPCA} ranges associated with regimes A, R, and G. The date above each plot refers to the year of the Jan of the corresponding winter.

North America sector resemble the positive and negative phases of the PNA pattern, respectively, this change in occupation statistics is consistent with the well-documented Northern Hemisphere extratropical response to ENSO events (e.g., Trenberth et al. 1998). The effect of ENSO on the PDF of $\lambda_{\mathrm{CPCA}}(t_n)$ is consistent with Palmer's (1999) hypothesis that the response of the atmosphere to external forcing is a change in the occupation frequencies of internally generated regimes and not in the structure of the regimes.

It is of course possible that the changes in the PDF of $\lambda_{\mathrm{CPCA}}(t_n)$ displayed in Fig. 8 result simply from sampling fluctuations. To assess the statistical significance of the changes in the PDF, we adopted the null hypothesis that the PDF associated with El Niño (La Niña) winters could have been produced by any random set of 11 (6) winters. This null hypothesis was tested using a bootstrap procedure, in which 5000 sets of 11 winters for El Niño and 6 for La Niña were drawn randomly (with replacement) from the set of 40 full winters. For

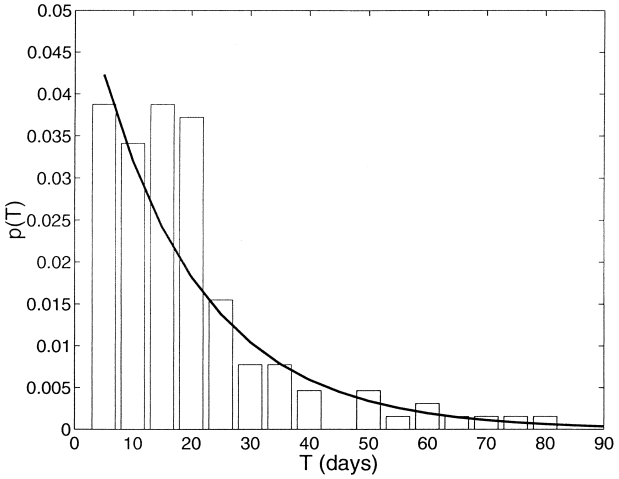

FIG. 5. Histogram estimate of the probability distribution $p(T)$ of regime residence times, T, for regimes A, R, and G. The thick line is the least squares best fit of $p(T)$ to the exponential distribution $(1/\tau)\exp(-T/\tau)$.

each of the 5000 sets the number of days falling into regimes A, R, and G was calculated. This analysis demonstrates that the increased occupation frequency of regimes R and A during El Niño and La Niña events, respectively, is significant at the 95% and 99% confidence levels. The decreased occupation frequency of regime A during El Niño years is marginally significant, with a 90% confidence level. None of the other changes in occupation frequencies is particularly significant.

The effect of ENSO on the joint PDF of the leading two PCA modes of 500-hPa heights was considered by Corti et al. (1999), who compared the PDF estimated using all years of data with that estimated after removing all ENSO years from the dataset. They demonstrated that there was no shift in the positions of the regimes, and therefore that the regimes themselves were not produced by ENSO variability. However, they did not consider the joint PDFs associated with El Niño and La Niña years and were thus not able to note the distinct changes in occupation statistics described above.

Besides interannual variability, the regime occupation frequencies displayed in Fig. 7 also display interdecadal trends. In particular, regime G is more frequently occupied in the first half of the record than in the second. The downward trend in the population of cluster G was noted by Corti et al. (1999). However, they also noted a downward and an upward trend in the populations of regimes A and R, respectively, which are not obvious in the time series presented in Fig. 7.

In short data records such as the one considered, it is difficult to differentiate with confidence between genuine trends and apparent trends generated by sampling fluctuations. It was demonstrated in Molteni and Corti (1998) that internal dynamics alone can induce substantial low-frequency variability in regime occupation statistics. However, the downward trend in the occupation frequency of regime G is interesting in light of the GCM study of MFF, as will be discussed later.

4. Analysis of stratospheric geopotential heights

Figure 9 displays the spatial structures of the two leading PCA modes of the Z_{20} field, explaining, respectively, 44% and 21% of the variance, along with an estimate of the joint PDF of the associated time series. This figure demonstrates that the joint PDF of the two time series deviates markedly from bivariate Gaussianity. The time series associated with mode 1 displays a pronounced positive skewness. Furthermore, the pair of time series are clearly not independent (although they are uncorrelated): the central peak of the joint distribution is roughly ellipsoidal, with a major axis aligned at roughly $-45°$ to the positive principal component-(PC) 1 axis.

Figure 10 displays a plot of the 1D NLPCA approximation to Z_{20}, $\hat{Z}_{20}(t_n)$, in the space of the leading two PCA modes. Projections of $\hat{Z}_{20}$ onto higher PCA modes are negligible. The state space structure of $\hat{Z}_{20}$ is substantially different than those of the 1D NLPCA approximations of the tropospheric fields. Where the tropospheric NLPCA approximations are U shaped, $\hat{Z}_{20}$ is composed of three straight branches. We will denote the leftmost branch in Fig. 10 as V, and the rightmost as MjW. As in Fig. 2, a plot of the difference between the joint distribution of the two PCA modes and the product of the marginals, $p(\mathrm{PC}_1, \mathrm{PC}_2) - p(\mathrm{PC}_1)p(\mathrm{PC}_2)$, is also contoured in Fig. 10. The difference is characterized by two positive regions separated by a strongly negative region. Two of the branches of $\hat{Z}_{20}$ lie along the preferred regions of state space, while the third connecting branch crosses the unpreferred region.

Figure 11 displays an estimate of the PDF of the time series, $\lambda_{20}(t_n)$, associated with $\hat{Z}_{20}(t_n)$. This PDF is characterized by two distinct peaks: the larger population with lower $\lambda_{20}(t_n)$ values lives on branch V, while the smaller population with higher $\lambda_{20}(t_n)$ values lives on branch MjW. The region of low values of the PDF corresponds to the intermediate joining branch. The triangles in Fig. 11 denote the values of $\lambda_{20}(t_n)$ at which the branches meet. Inspection of the PDF of $\lambda_{20}(t_n)$ indicates that the population on branch V is itself bimodal. These secondary peaks are robust to a broad range of smoothing parameters used in the estimation of the PDF of λ_{20}. The 1D NLPCA description of Z_{20} then indicates the existence of two major branches, denoted V and MjW, the first of which is composed of two weakly separated regimes, denoted C_1 and M. The branch MjW is composed of a single regime, which will itself be denoted MjW. The reasons for the names given to these regimes will become clear when the full time series and associated spatial patterns are presented. Note that the peaks of λ_{20} occur near regions of state space in which the difference between the joint PDF of the

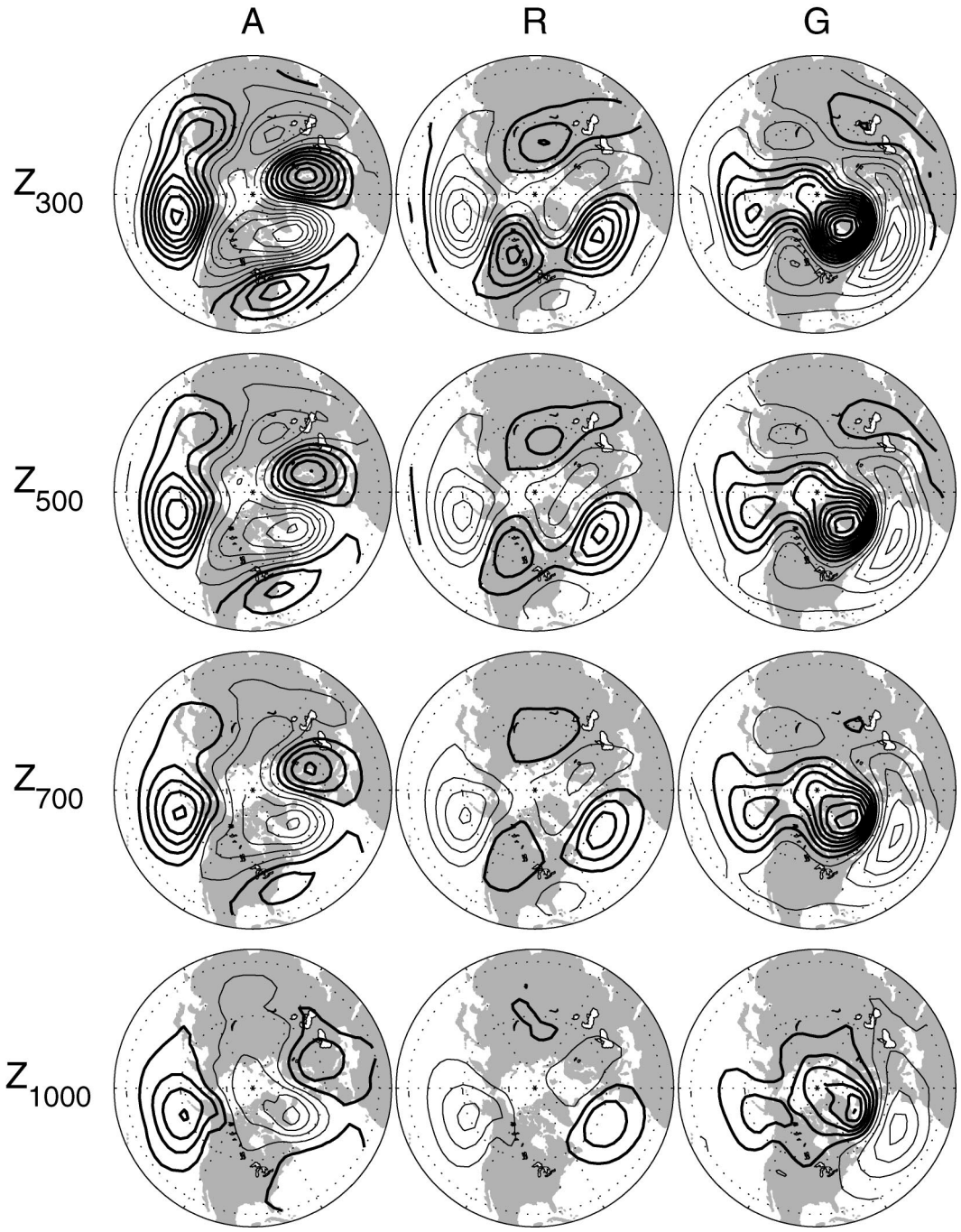

FIG. 6. Geopotential height anomalies corresponding to the regimes A, R, and G of $\hat{Z}_{\mathrm{CPCA}}(t_n)$ at 1000, 700, 500, and 300 hPa. Bold contours are positive and thin contours are negative. Contour interval is (. . . , −30, −10, 10, 30, . . .) m.

two PCA modes and the product of the marginals displays local maxima.

A plot of $\lambda_{20}(t_n)$ for each full winter in the observational record is presented in Fig. 12. The more populous branch is designated by V to indicate that the atmosphere generally displays vacillatory behavior when its state space representation moves along this branch. The atmosphere spends most of the time moving within V, sometimes slowing down in the vicinity of regimes C_1 and M. Evident are episodes in which the system resides for an extended period in regime C_1 (e.g., 1972) or regime M (e.g., 1965). Occasionally, the system jumps to branch MjW, on which it resides for a time on the order of a month before returning to branch

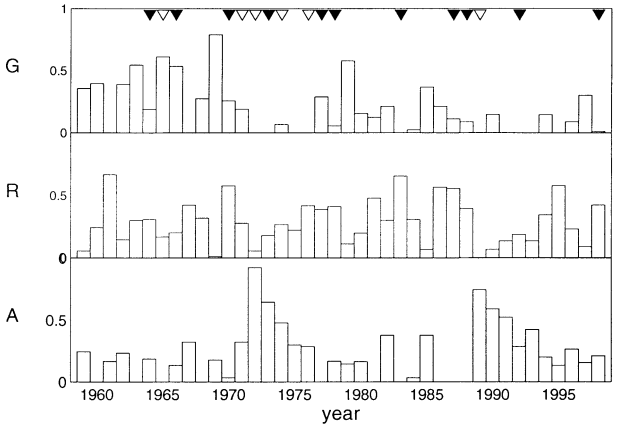

FIG. 7. Annual occupation frequencies of regimes A, R, and G, for each winter in the observational record. The solid and open triangles denote El Niño and La Niña years, respectively.

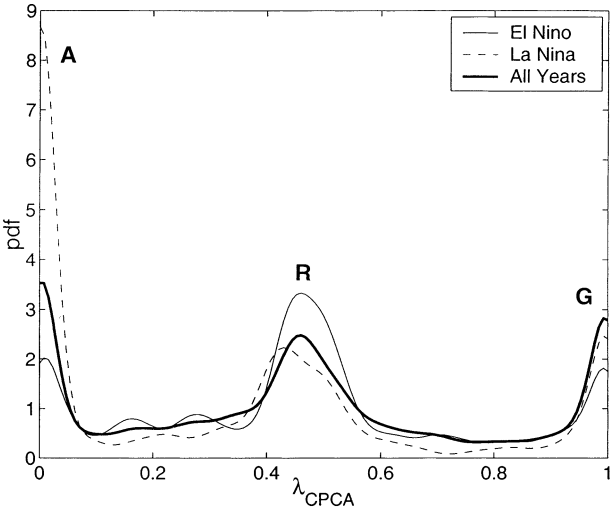

FIG. 8. Gaussian kernel estimates of the PDF of $\lambda_{\mathrm{CPCA}}(t_n)$ for El Niño winters (thin solid line), La Niña winters (thin dashed line), and all winters (thick solid line).

V. It is apparent from Fig. 12 that the trajectory through regime MjW follows one of two distinct patterns: gradual rise and decline (e.g., 1968, 1985), or extremely rapid rise and gradual decline (e.g., 1970, 1977). As was the case with $\lambda_{\mathrm{CPCA}}(t_n)$, two clear ranges of timescales are apparent: the shorter timescale, on the order of days, describes transitions between the branches V and MjW, while the longer timescale characterizes the occupation time of either branch.

To illustrate the spatial patterns associated with $\hat{Z}_{20}$, we will consider the five representative points indicated in Figs. 10 and 11: C_2, C_1, M, MnW, and MjW. Points C_1, M, and MjW lie in the middle of the associated regimes, and points C_2 and MnW lie on the flanks of the PDF on branch V. Figure 13 displays composite maps of the 20-hPa geopotential height and temperature fields for those days in which the system is near these characteristic points. It is clear from Fig. 10 that regime M lies very close to the climatological mean, thus its designation by M. Relative to regime M, regime C_1 is characterized by enhanced zonal flow, reduced polar temperatures, a northward shift of the vortex center to directly over the pole, a more elliptical vortex, and a westward realignment of the major axis of the vortex along the 90°E–90°W line of longitude. These features are even more pronounced at the point C_2. The flow at MnW is characterized by a somewhat reduced zonal flow, a warmer pole, a shift of the vortex center away from the pole, a less elliptical vortex, and an eastward shift of the vortex axis, relative to the climatological mean. Finally, regime MjW exhibits pronounced reductions of the strength of the zonal flow and the latitudinal temperature gradient. Figure 14 displays estimates of the joint PDFs of $\lambda_{20}(t_n)$ with the zonal-mean geostrophic zonal wind at 60°N and with the zonal-mean temperature gradient calculated between 60°N and the pole. Clearly, regime MjW is associated with a dramatic reduction of the strength of the westerly flow, or even a reversal of direction, at 20 hPa in high latitudes. As well, there is a dramatic reduction or reversal of the temperature gradient between 60°N and the pole. Such attenuation or reversal of the high-latitude stratospheric westerlies and meridional temperature gradient is characteristic of major sudden stratospheric warmings, and regime MjW is therefore interpreted as representing such events. The region around MnW is interpreted as being characteristic of minor stratospheric warmings, in which there is a more pronounced reduction in the zonal-mean meridional temperature gradient than in the zonal-mean zonal wind. Note that these definitions of major and minor warmings differ from the standard World Meteorological Organization (WMO) definition; all major warming events identified by the WMO definition correspond to major warmings in the present definition, but not vice versa.

Our analysis has indicated the existence of three preferred regimes of circulation in both the stratosphere (C_1, M, and MjW) and the troposphere (G, R, and A). A natural question arises as to the relation between these sets of regimes. Figure 15 contours an estimate of the joint PDF of $\lambda_{\mathrm{CPCA}}(t_n)$ and $\lambda_{20}(t_n)$. Inspection of this figure indicates that stratospheric regime MjW events occur most often in association with tropospheric regime G events (and only rarely when the troposphere is in regime R or A) while the reverse is not true. Stratospheric regimes M and C_1 events also occur when the troposphere is in regime G, with M events being more common. When the troposphere is in regime R, the stratosphere is most likely to be found in regime M, and when the troposphere is in regime A, the stratosphere is most likely to be in regime C_1. Figure 15 thus demonstrates that there are clear relationships between the tropospheric and stratospheric regimes, although these relationships are not simple. Note as well that regimes

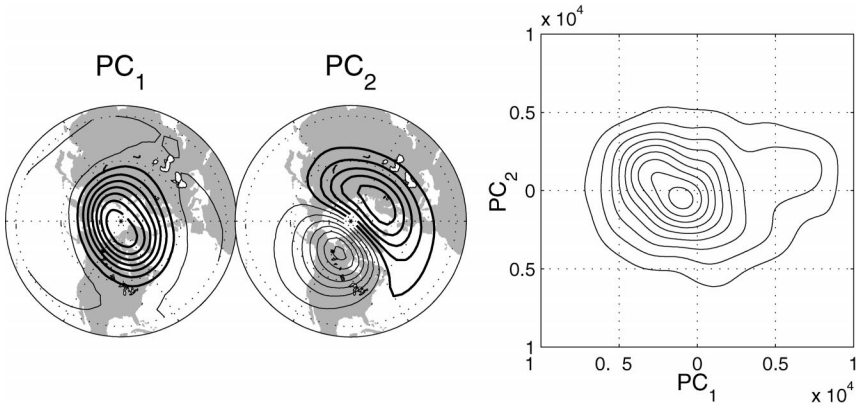

FIG. 9. Spatial structure of the two leading PCA modes of the Z_{20} field (thick lines are positive contours, thin lines are negative; contour interval is . . . , −0.03, −0.01, 0.01, . . .) and a Gaussian kernel estimate of the joint PDF of the associated time series (contour interval is 2×10^{-9}). The estimate was made with the smoothing parameter $h = 1000$.

C_1 and M appear to be more clearly separated in this figure than in the PDF of λ_{20} alone (Fig. 11).

As has been noted in a number of studies (e.g., Chaffey and Fyfe 2001), stratospheric sudden warmings have been less common in the 1990s than in earlier decades. Figure 16 displays the fraction of days spent in branch MjW for each winter of the observational record. There is an evident reduction of the frequency of MjW events in the second half of the record, as compared to the first half. This trend is particularly interesting in light of the

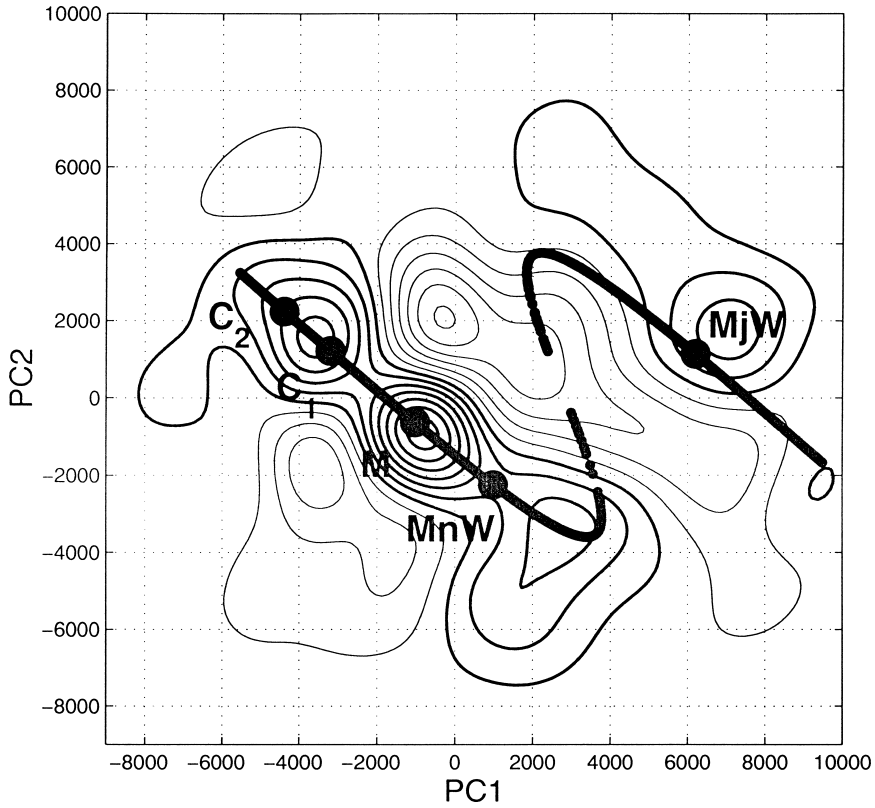

FIG. 10. Plot of the 1D NLPCA approximation $\hat{Z}_{20}$ (thick curve) in the space spanned by the leading two PCA modes. The circles represent the state space positions of points C_2, C_1, M, MnW, and MjW in Fig. 11. Also contoured is the difference between the joint PDF $p(PC_1, PC_2)$ and the product of the marginals $p(PC_1)\,p(PC_2)$. Thick contours are positive, while thin contours are negative. Contour interval is $(\ldots, -0.75, -0.25, 0.25, \ldots) \times 10^{-9}$.

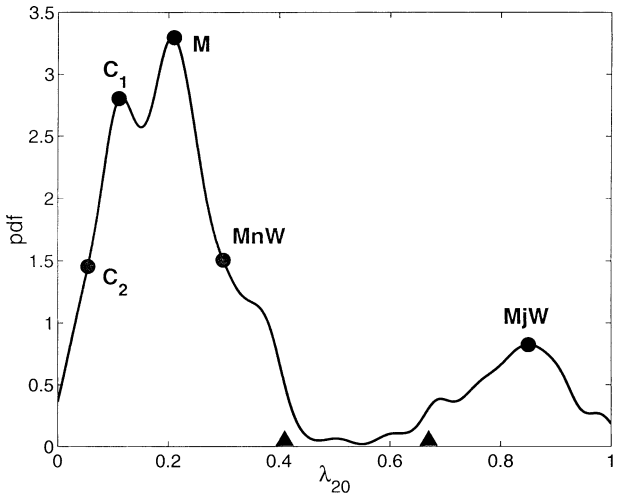

FIG. 11. Estimate of the PDF of $\lambda_{20}(t_n)$, made with a smoothing parameter, $h = 0.025$. The triangles mark the values of $\lambda_{20}(t_n)$ at which the branches of $\hat{Z}_{20}$ meet.

connection of stratospheric regime MjW with tropospheric regime G, and the downward trend in frequency of occupation of this tropospheric regime. Again, in both cases the trend could simply be due to sampling fluctuations, because the records are short. Nonetheless, one must note the connection with volcanic eruptions. There have been three strong eruptions of tropical volcanos since 1959. From the weakest to the strongest, these were Agung (1963), El Chicon (1982), and Pinatubo (1991). These strong tropical eruptions created vertical plumes that injected sulfate aerosols into the lower stratosphere. Absorption of radiation by these aerosols increased the pole-to-equator temperature gradients, which resulted in a strengthened stratospheric polar vortex (Robock 2000). This volcanic radiative forcing increases the likelihood of finding the stratospheric state on branch V and, consequently, prevents the development of MjW events for a few winters after the eruptions (see Fig. 12). Winters 1964/65 after Agung, 1983/84 after El Chicon, and 1992/93, 1993/94 after Pinatubo are examples of this phenomenon. Internal variability on interannual timescales is probably responsible for the 1974–76 and 1995–97 stretches without major stratospheric sudden warmings. To test the relationship between major volcanic eruptions and the absence of regime MjW events, the following bootstrap test was used. From the full record of 40 winters, 1000 sets of three nonoverlapping 2-yr periods were randomly selected. From this set, only on five occasions were all three 2-yr periods free of regime MjW events. This strongly suggests that the relationship between major volcanic eruptions and the depopulation of regime MjW is not an artifact of chance. In the end, it still remains to be shown (Pawson et al. 2000) whether the decreasing trend displayed in Fig. 16 is due to forcing by volcanic aerosols, global warming, polar ozone depletion, the 11-yr solar cycle, internal variability, or a combination of these causes.

Three stratospheric regimes, similar to those we have identified, were also noted in the study by Pierce and Fairlie (1993). Their regimes 2 and 1b strongly resemble our regimes M and C_2, while their regime 1a is similar to our regime MjW in that it corresponds to a strong reduction in the midstratospheric westerlies, although it contains a stronger zonal wavenumber 2 component than our regime MjW. A basic difference between the study of Pierce and Fairlie and the present one is that here we identify regimes C_2 and M as being part of a single vacillatory branch, while Pierce and Fairlie group C_2 and MjW together. The NLPCA description of the primary mode of stratospheric variability as fluctuations in the shape and location of the polar vortex is complementary to the description arising from the study of Waugh and Randel (1999), which employed a diagnostic of polar vortex ellipticity. Their study identified two broad classes of stratospheric vortex states, denoted D (''distorted'') and Q (''quiescent''). The two classes were distinguished by differences in vortex ellipticity, eccentricity, major axis alignment, and location of the center relative to the pole. The D (Q) states of Waugh and Randel are highly reminiscent of the MnW (C_1 and C_2) states of the present study. Presumably, MjW events were not highlighted by the diagnostic used in Waugh and Randel because the polar vortex collapses during major warmings.

The connection between tropospheric blocking and stratospheric sudden warmings, based on synoptic criteria, was noted by Quiroz (1986). A more general study of the covariability of the tropospheric and stratospheric circulations was carried out by Perlwitz and Graf (1995), using canonical correlation analysis (CCA). The leading CCA mode of their analysis indicates a connection between an NAO-like pattern in the troposphere and a zonally symmetric anomaly pattern in the stratosphere, centered over the pole. The second mode correlates a tropospheric PNA-like pattern with a stratospheric dipole pattern with oppositely signed centers of action over northern Canada and northeastern Siberia. Because of their use of a linear diagnostic, this relationship between stratospheric vortex strength and the NAO is symmetric: positive (negative) NAO episodes are associated with an intensification (weakening) of the vortex. In this study, we do not find that the mirror-image patterns of regimes MjW and G are preferred structures of the data.

The existence of multiple regimes of circulation over a broad range of tropospheric forcing values is a generic feature of simple analytic models of stratospheric variability (e.g., Holton and Mass 1976; Yoden 1987,1990; Christiansen 2000). What is unclear from these models is the mechanism responsible for transitions between different basins of attraction. One possibility is that changes in tropospheric forcing move the system beyond bifurcation points at which one of the regimes ceases to exist, potentially inducing a transition. An-

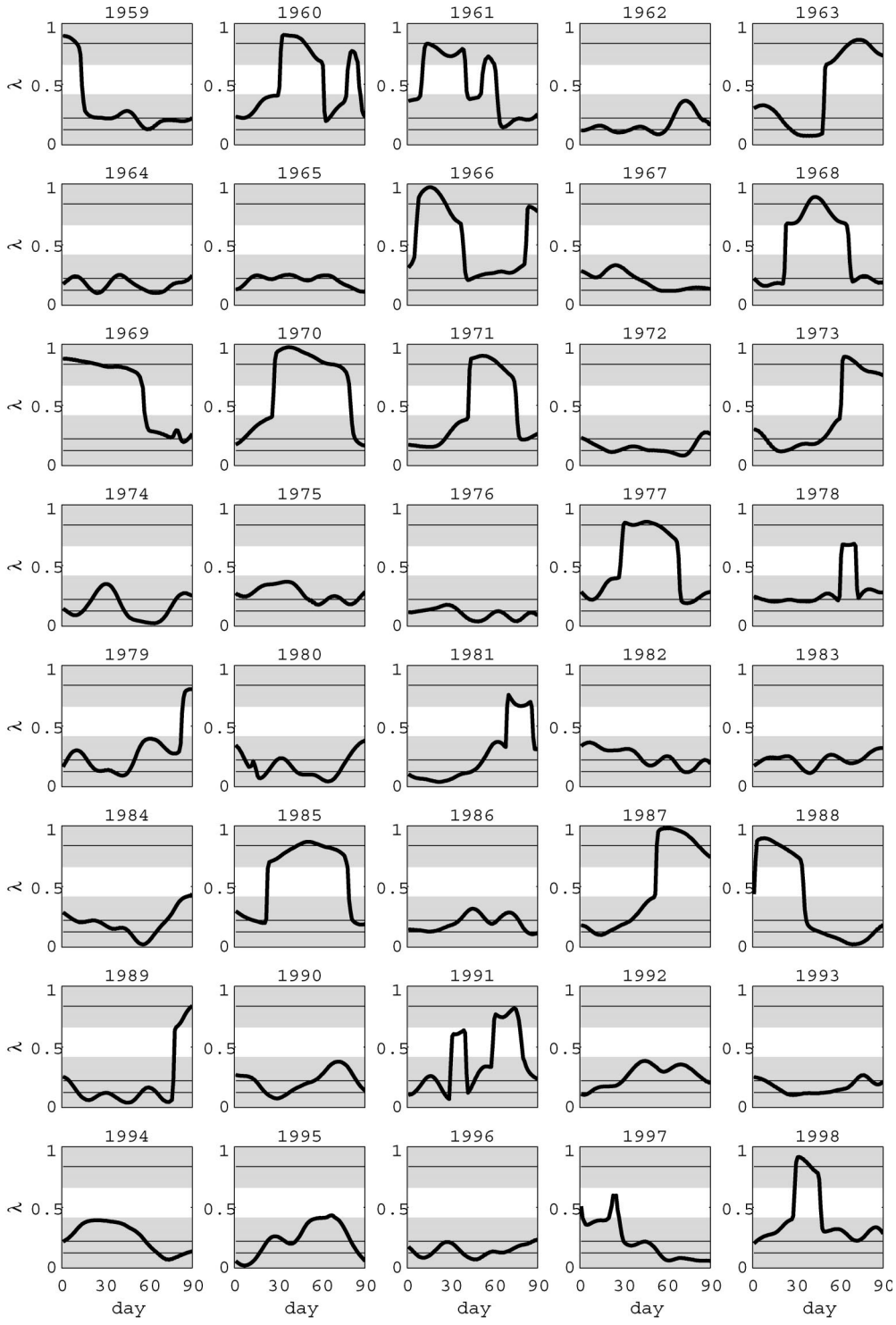

FIG. 12. Plot of $\lambda_{20}(t_n)$ for each full winter in the observational record (thick curve). The shaded regions denote the λ_{20} ranges on branches V and MjW, and the thin lines denote the positions of the peaks C_1, M, and MjW.

other possibility is that fluctuations in planetary and gravity wave forcing at the tropopause induce hopping between regimes. In fact, both of these possibilities could be at work in regime transitions. Further comparison between the dynamics of simple mechanistic models and the stratospheric regimes found in the observations may help to distinguish between these mechanisms.

5. Summary and conclusions

In this study we have extended the analysis of the wintertime NH 500-hPa height field presented in MPF to the entire tropospheric column and to the 20-hPa height field in the stratosphere. A combined analysis of four tropospheric geopotential height fields demonstrates that the three regimes identified in MPF at 500 hPa are coherent throughout the troposphere, displaying a strong equivalent barotropic structure. The occupation statistics of these three regimes are influenced by ENSO variability, such that El Niño and La Niña events bias the distribution toward those regimes whose anomalies over the Pacific–North American sector resemble the positive and negative phases of the PNA pattern, respectively. Furthermore, the occupation frequency of one regime demonstrates a notable downward trend over the period of the observations.

The 1D NLPCA approximation of the extratropical NH 20-hPa height field indicates that the stratosphere is characterized by two dominant circulation branches, the first of which consists of two regimes, the second of which consists of one. These regimes resemble those previously identified by Pierce and Fairlie (1993) using a zonal wave index. The more populous branch describes a vacillation in stratospheric polar temperatures and vortex structure; the other, which is occupied episodically, corresponds to stratospheric sudden warming events. The stratospheric and tropospheric regimes were shown to be related, such that the occupation of a given tropospheric regime makes more or less likely the occupation of the various stratospheric regimes and vice versa.

There are striking similarities and differences between the NLPCA approximations to monthly averaged NH sea level pressure and 500-hPa geopotential height fields from the CCCma GCM (MFF; Monahan 2000b), and those of the 10-day low-pass filtered observations. In both cases, multiple equivalent-barotropic regimes of circulation were identified in the troposphere. However, the observational data are characterized by three quasistationary regimes while the GCM output is characterized by one quasistationary and one vacillatory regime. The quasistationary regime identified in the GCM corresponds very closely to quasistationary regime G in the present model. Three possible reasons for the differences in regime structure are model error, sampling fluctuations, or effects due to the use of different temporal filters. A recent careful analysis of both model output and observations over a range of temporal filtering parameters (Fyfe et al., unpublished manuscript) strongly supports this third explanation for the differences between the results of MFF, and those of MPF and the present study.

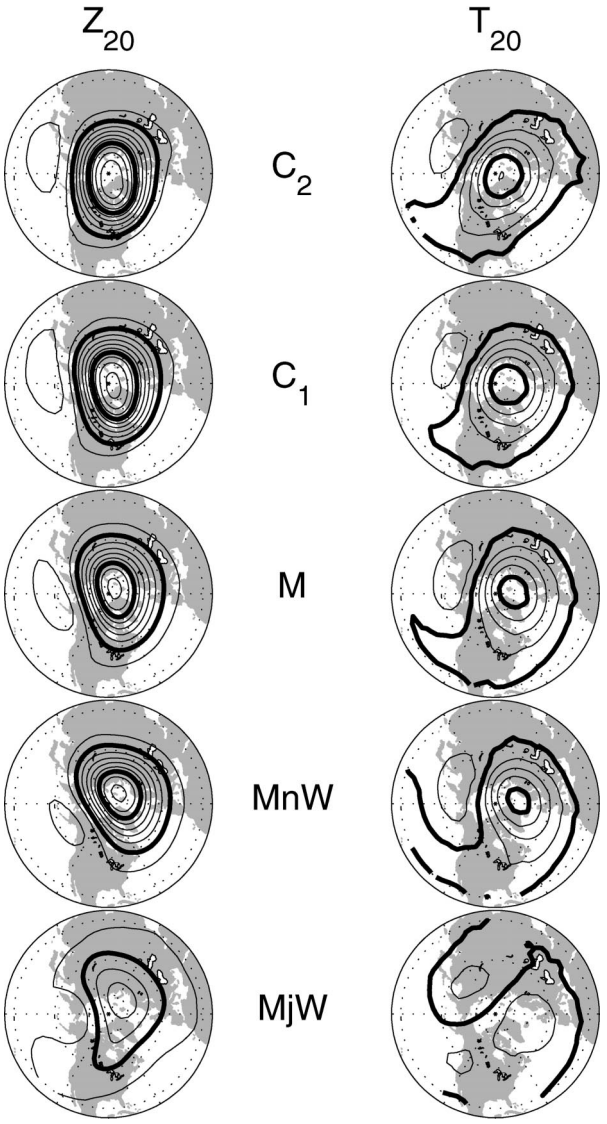

FIG. 13. The 20-hPa geopotential height and temperature fields corresponding to the points C_2, C_1, M, MnW, and MjW. For the height fields, the contour interval is 200 m and the contours at 25 (inner contour) and 26 km (outer contour) are in bold. For the temperature fields, the contour interval is 5 K and the contours at 200 (inner contour) and 220 K (outer contour) are in bold. Only the 26-km and 220-K contours appear in bold in the MjW fields.

A final comparison between the results of MFF and those of the present study is worth noting. As was mentioned above, the primary effect of anthropogenic forcing on atmospheric variability in the CCCma coupled GCM was the depopulation of the quasistationary regime, which strongly resembles regime G of the present study. In section 3, it was shown that the frequency of

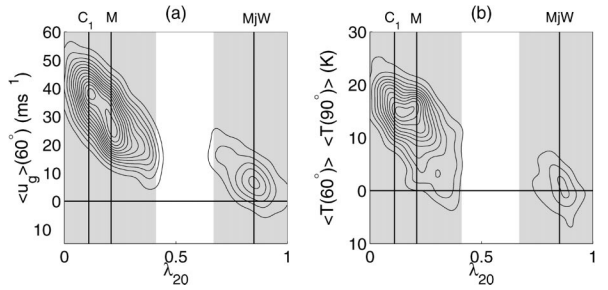

FIG. 14. (a) Joint PDF of $\lambda_{20}(t_n)$ and the zonal-mean geostrophic zonal wind at 60°N. Contour interval is 0.01. (b) Joint PDF of $\lambda_{20}(t_n)$ and the zonal-mean temperature gradient between 60° and 90°N. The shaded regions indicate the λ_{20} regions on V and MjW. The vertical lines denote the positions of peaks C_1, M, and MjW, and the horizontal line is the zero line.

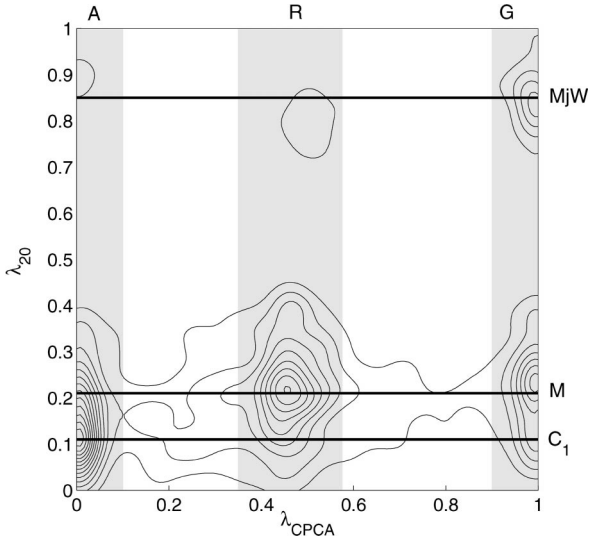

FIG. 15. Joint PDF of $\lambda_{\mathrm{CPCA}}(t_n)$ and $\lambda_{20}(t_n)$, estimated with a smoothing parameter $h = 0.03$. Contour interval is 1. The shaded regions indicate the λ_{CPCA} and λ_{20} regions corresponding to tropospheric regimes A, R, and G stratospheric branches V and MjW. The thick solid lines denote the λ_{20} values of the points C_1, M, and MjW.

occupation of regime G has been decreasing over the 40 years of the observational record. The correspondence between the observed regime trends and those predicted to result from anthropogenic forcing is intriguing. On the one hand, it seems to indicate that greenhouse gases forcing in the troposphere could explain the decreasing trend of G events. On the other hand, this trend could have its origin in the stratosphere. In section 4, we noted the strong connection between the MjW and G regimes. We also described how known forcing agents could be responsible for the decreasing occurrence of MjW events, which would then imply a similar trend in the frequency of occurrence of regime G. Of course, all these trends could simply be a result of internal low-frequency variability in the climate system.

The idea that extratropical NH LFV is dominated by the approximately zonally symmetric Arctic Oscillation, or annular mode, which is coherent from the surface to the upper stratosphere, has attracted considerable attention in recent years (e.g., Thompson and Wallace 1998, 2000; Baldwin and Dunkerton 1999; Shindell et al. 1999; Fyfe et al. 1999; Thompson et al. 2000; Wallace, 2000; Ambaum et al. 2001). This mode of variability is obtained as the 1D PCA approximation to the geopotential height field at one or more pressure levels. The connection between individual PCA modes and physical modes of variability is, however, unclear. It was demonstrated by North (1984) that individual PCA modes correspond to dynamical modes only for linear systems, whose associated dynamical operator commutes with its adjoint, driven by spatially incoherent noise. These are strong constraints, especially given that the basic equations of motion of fluid dynamics are strongly nonlinear. Deduction of dynamics from statistics is a delicate matter. Nevertheless, statistical analyses can help determine the class of dynamical systems that is consistent with a given dataset. In particular, a multimodal dataset is not consistent with linear dynamics. It is clear from Figs. 2 and 10 that the leading PCA approximation, the AO, runs between the regimes in such a way as to minimize the squared error. In this sense, the AO is the optimal linear approximation to the actual underlying nonlinear distribution. This suggests that the AO is not a dynamical mode of variability. We do not suggest that the 1D NLPCA approximation is itself a dynamical mode independent of other degrees of freedom; it is simply a more faithful low-dimensional representation of the nonlinear structure of the data than is the PCA approximation.

Another difference between the results of this study and the annular mode paradigm is the distinction between tropospheric and stratospheric modes of variability. The annular mode paradigm proposes that the dominant structures of variability in the troposphere and the stratosphere are essentially the same: the AO. In this analysis, distinctly different low-dimensional structures of variability emerge in the troposphere and the stratosphere. These structures are not unrelated, as the joint PDF of the time series $\lambda_{\mathrm{CPCA}}(t_n)$ and $\lambda_{20}(t_n)$ (Fig. 15) demonstrates, but they are different.

The statistical analysis presented in this study indicates that the nonlinearities in the equations of atmospheric motion manifest themselves in the existence of a number of preferred quasistationary circulation regimes. This inherently nonlinear structure in the distri-

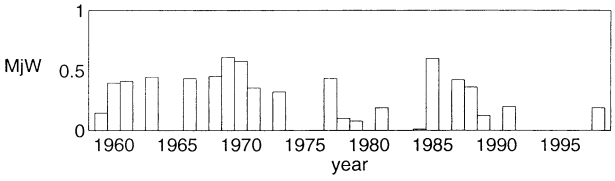

FIG. 16. Fraction of days spent on $\hat{Z}_{20}$ branch MjW for each complete winter of the observational record.

bution of low-frequency variability has bearing on the use of linear stochastic models to describe the second moments of extratropical LFV (e.g., Newman et al. 1997). The results also suggest that nonlinearities in the dynamics do not act as simply as turbulent fluctuations and enhanced damping. Therefore, simple theories of the extratropical LFV will have to account for the existence of these preferred regimes of circulation.

Acknowledgments. The authors would like to thank Bin Yu and Jian Sheng for their helpful comments on an early draft of this paper. We would also like to thank the two anonymous referees for their helpful comments, which improved the manuscript. A. Monahan was supported by DFG Schwerpunktprogramm ''Interagierende stochastische Systeme von hoher Komplexität,'' and A. Monahan and L. Pandolfo were supported by the Natural Sciences and Engineering Research Council of Canada and by the Crisis Points Group of the Peter Wall Institute for Advanced Studies.

REFERENCES

Aires, F., A. Chedin, and J.-P. Nadal, 2000: Independent component analysis of multivariate time series: Application to the tropical SST variability. *J. Geophys. Res.,* **105,** 17 437–17 455.

Ambaum, M. H. P., B. J. Hoskins, and D. B. Stephenson, 2001: Arctic Oscillation or North Atlantic Oscillation? *J. Climate,* **14,** 3495–3507.

Baldwin, M. P., and T. J. Dunkerton, 1999: Propagation of the Arctic Oscillation from the stratosphere to the troposphere. *J. Geophys. Res.,* **104,** 30 937–30 946.

Barnston, A. G., and R. E. Livezey, 1987: Classification, seasonality, and persistence of low-frequency atmospheric circulation patterns. *Mon. Wea. Rev.,* **115,** 1083–1126.

Baur, F., 1931: Die Formen der atmosphärischen Zirculation in der gemässigten Zone. *Beitr. Geophys.,* **34,** 264–309.

Chaffey, J. D., and J. C. Fyfe, 2001: Arctic polar vortex variability in the Canadian Middle Atmosphere Model. *Atmos.–Ocean,* **39,** 457–469.

Charney, J. G., and J. G. DeVore, 1979: Multiple flow equilibria in the atmosphere and blocking. *J. Atmos. Sci.,* **36,** 1205–1216.

Cheng, X., and J. M. Wallace, 1993: Cluster analysis of the Northern Hemisphere wintertime 500-hPa height field: Spatial patterns. *J. Atmos. Sci.,* **50,** 2674–2696.

Christiansen, B., 2000: Chaos, quasiperiodicity, and interannual variability: Studies of a stratospheric vacillation model. *J. Atmos. Sci.,* **57,** 3161–3173.

Corti, S., F. Molteni, and T. Palmer, 1999: Signature of recent climate change in frequencies of natural atmospheric circulation regimes. *Nature,* **398,** 799–802.

Fyfe, J. C., G. J. Boer, and G. M. Flato, 1999: The Arctic and Antarctic Oscillations and their projected changes under global warming. *Geophys. Res. Lett.,* **26,** 1601–1604.

Gardiner, C. W., 1997: *Handbook of Stochastic Methods for Physics, Chemistry, and the Natural Sciences.* Springer, 442 pp.

Hannachi, A., and A. O'Neill, 2001: Atmospheric multiple equilibria and non-Gaussian behaviour in model simulations. *Quart. J. Roy. Meteor. Soc.,* **127,** 939–958.

Holton, J. R., and C. Mass, 1976: Stratospheric vacillation cycles. *J. Atmos. Sci.,* **33,** 2218–2225.

Hsu, C. J., and F. Zwiers, 2001: Climate change in recurrent regimes and modes of atmospheric variability. *J. Geophys. Res.,* **106** (D17), 20 145–20 159.

Kalnay, E., and Coauthors, 1996: The NCEP/NCAR 40-year Reanalysis Project. *Bull. Amer. Meteor. Soc.,* **77,** 437–471.

Kimoto, M., and M. Ghil, 1993: Multiple flow regimes in the Northern Hemisphere winter. Part I: Methodology and hemispheric regimes. *J. Atmos. Sci.,* **50,** 2625–2643.

Molteni, F., and S. Corti, 1998: Long-term fluctuations in the statistical properties of low-frequency variability: Dynamical origin and predictability. *Quart. J. Roy. Meteor. Soc.,* **124,** 495–526.

Monahan, A. H., 2000a: Nonlinear principal component analysis by neural networks: Theory and application to the Lorenz system. *J. Climate,* **13,** 821–835.

——, 2000b: Nonlinear principal component analysis of climate data. Ph.D. thesis, University of British Columbia, Vancouver, BC, Canada, 159 pp. [Available online at http://web.uvic.ca/~monahana/monahan.html.]

——, 2001: Nonlinear principal component analysis: Tropical Indo-Pacific sea surface temperature and sea level pressure. *J. Climate,* **14,** 219–233.

——, J. C. Fyfe, and G. Flato, 2000: A regime view of Northern Hemisphere atmospheric variability and change under global warming. *Geophys. Res. Lett.,* **27,** 1139–1142.

——, L. Pandolfo, and J. C. Fyfe, 2001: The preferred structure of variability of the Northern Hemisphere atmospheric circulation. *Geophys. Res. Lett.,* **28,** 1019–1022.

Namias, J., 1950: The index cycle and its role in the general circulation. *J. Meteor.,* **7,** 130–139.

Newman, M., P. D. Sardeshmukh, and C. Penland, 1997: Stochastic forcing of the wintertime extratropical flow. *J. Atmos. Sci.,* **54,** 435–455.

North, G. R., 1984: Empirical orthogonal functions and normal modes. *J. Atmos. Sci.,* **41,** 879–887.

Palmer, T., 1999: A nonlinear dynamical perspective on climate prediction. *J. Climate,* **12,** 575–591.

Pandolfo, L., 1993: Observational aspects of the low-frequency intraseasonal variability of the atmosphere in middle latitudes. *Advances in Geophysics,* Vol. 34. Academic Press, 93–174.

Pawson, S., and Coauthors, 2000: The GCM-Reality Intercomparison Project for SPARC (GRIPS): Scientific issues and initial results. *Bull. Amer. Meteor. Soc.,* **81,** 781–796.

Perlwitz, J., and H.-F. Graf, 1995: The statistical connection between tropospheric and stratospheric circulation of the Northern Hemisphere in winter. *J. Climate,* **8,** 2281–2295.

Pierce, R. B., and T. D. A. Fairlie, 1993: Observational evidence of preferred flow regimes in the Northern Hemisphere winter stratosphere. *J. Atmos. Sci.,* **50,** 1936–1949.

Quiroz, R. S., 1986: The association of stratospheric warmings with tropospheric blocking. *J. Geophys. Res.,* **91,** 5277–5285.

Renwick, J. A., and J. M. Wallace, 1996: Relationships between North Pacific wintertime blocking, El Niño, and the PNA pattern. *Mon. Wea. Rev.,* **124,** 2071–2076.

Robock, A., 2000: Volcanic eruptions and climate. *Rev. Geophys.,* **38,** 191–219.

Shindell, D. T., R. L. Miller, G. A. Schmidt, and L. Pandolfo, 1999: Simulation of recent northern winter climate trends by greenhouse-gas forcing. *Nature,* **399,** 452–455.

Smyth, P., K. Ide, and M. Ghil, 1999: Multiple regimes in Northern Hemisphere height fields via mixture model clustering. *J. Atmos. Sci.,* **56,** 3704–3723.

Sutera, A., 1986: Probability density distribution of large-scale atmospheric flow. *Advances in Geophysics,* Vol. 29. Academic Press, 227–249.

Thompson, D. W., and J. M. Wallace, 1998: The Arctic Oscillation signature in the wintertime geopotential height and temperature fields. *Geophys. Res. Lett.,* **25,** 1297–1300.

——, and ——, 2000: Annular modes in the extratropical circulation. Part I: Month-to-month variability. *J. Climate,* **13,** 1000–1016.

——, ——, and G. C. Hegerl, 2000: Annular modes in the extratropical circulation. Part II: Trends. *J. Climate,* **13,** 1018–1036.

Trenberth, K. E., G. W. Branstator, D. Karoly, A. Kumar, N.-C. Lau, and C. Ropelewski, 1998: Progress during TOGA in understand-

ing and modeling global teleconnections associated with tropical sea surface temperatures. *J. Geophys. Res.*, **103,** 14 291–14 324.
Wallace, J. M., 2000: North Atlantic Oscillation/Annular Mode: Two paradigms—One phenomenon. *Quart. J. Roy. Meteor. Soc.*, **126,** 791–806.
——, and D. S. Gutzler, 1981: Teleconnections in the geopotential height field during the Northern Hemisphere winter. *Mon. Wea. Rev.*, **109,** 784–812.
——, G.-H. Lim, and M. Blackmon, 1988: Relationship between cyclone tracks, anticyclone tracks, and baroclinic waveguides. *J. Atmos. Sci.*, **45,** 439–462.
——, C. Smith, and C. S. Bretherton, 1992: Singular value decomposition of wintertime sea surface temperature and 500-mb height anomalies. *J. Climate*, **5,** 561–576.
Waugh, D. W., and W. J. Randel, 1999: Climatology of Arctic and Antarctic polar vortices using elliptical diagnostics. *J. Atmos. Sci.*, **56,** 1594–1613.
Yoden, S., 1987: Bifurcation properties of a stratospheric vacillation model. *J. Atmos. Sci.*, **44,** 1723–1733.
——, 1990: An illustrative model of seasonal and interannual variations of the stratospheric circulation. *J. Atmos. Sci.*, **47,** 1845–1853.